Effect of Preparation Temperature on the Microstructure and Physical Properties of Chemically Deposited SnO_2 Thin Films

Ibtihaj Abdulsamad Sabri[1*] , Jamal Fadhil Mohammad[1]

[1]Department of Physics, College of Education for Pure Science, University Of Anbar, Anbar, Ramadi, Iraq

*Corresponding Author Email: ibt22u3016@uoanbar.edu.iq

Abstract

In this work, tin dioxide (SnO_2) thin films were prepared by thermochemical decomposition method with different deposition temperature (325°C to 375°C)) using the precursor concentrations of 0.02 M. X-ray diffraction (XRD), scanning electron microscopy (SEM), atomic force microscopy (AFM), UV–Visible spectroscopy, and Hall effect measurements were conducted on films, to comprehensively evaluate their structural, optical, and electrical properties and the effect of temperature. Increasing deposition temperature leads initially to improved crystallinity and surface uniformity with optimal microstructural quality being reached at 350 °C with subsequent degradation at 375 °C due to increased lattice disorder and increasing lattice strain. The enhanced transmittance with and widening of the band gap (with increasing temperature) due to reduced film thickness and porosity were supported by optical characterization. Electrical measurements indicate that films fabricated at 350 °C possess the highest carrier mobility and electrical conductivity despite low carrier concentrations. These results show that the best compromise between structural order and charge transport efficiency is achieved at 350 °C. This study shows great promise in understanding how to tune the physical properties of SnO_2 thin films by controlling the thermal process, and their potential for opto-electronic and sensing applications.

Keywords: Tin dioxide (SnO_2); thin films; deposition temperature; optical transparency; carrier mobility; thermochemical decomposition; structural characterization

1. Introduction

SnO_2, with a wide direct band gap (3.6–4.0 eV), is a characteristic n-type semiconductor material that exhibits chemical stability, visible range transparency and good electrical conductivity [1-3].

Because of these properties, it can be used in gas sensors, solar cells, transparent electrodes, UV detectors and other optoelectronic devices [4, 5]. The structural, morphological, optical, and electrical properties of SnO_2 thus critically are often determined by the synthesis technique and processing parameters, and consequently affect the performance of SnO_2 in such applications [6].

Thermochemical deposition method, spray pyrolysis, is an efficient, low cost and scalable route to fabricate high quality SnO_2 thin films over large areas [7, 8]. It provides fine control over the film's characteristics, by modulation of parameters like precursor concentration, spray rate and most importantly substrate temperature [9]. Grain size, crystallinity, substrate temperature, porosity, film thickness and charge carrier behaviour are directly dependent on substrate temperature in particular [10, 11].

Increasing substrate temperature is a well-known fact and has been reinforced by recent studies of leading to better crystallinity, better grain growth, higher carrier mobility [12], and higher optical transparency [13]. Moreover, electronic band structure and defect states are modulated by the temperature, which results in the variations in the photoluminescence and photoconductivity performance [14]. Significant impact of substrate temperature on the incorporation and activation of dopants like Ni or Bi on doped SnO_2 film properties and thin film conductivity, Seebeck coefficient and optical bandgap is demonstrated through investigations on doped SnO_2 films [15, 16].

In addition, composite and hybrid SnO_2 systems display major improvement in temperature dependent sensor response, uniformity and crystallinity behavior [17, 18] and therefore require development of thermal conditions for advanced functionality.

Although these advancements have taken place, very few studies have systematically studied the combined effect of substrate temperature on these structural, morphological, optical and electrical properties of undoped SnO_2 thin films deposited by spray pyrolysis at low precursor concentrations. The relationship between temperature, grain growth, carrier transport and band gap tuning are still poorly understood and with complex interdependence.

The objective of this study is to fill this gap by a detailed evaluation of SnO2 thin films deposited by spray pyrolysis at low precursor concentration (0.02 M) on different substrate temperatures (325 °C, 350 °C and 375 °C). X-ray diffraction (XRD), scanning electron microscopy (SEM),

atomic force microscopy (AFM), UV–Vis spectroscopy and Hall effect measurements were used to characterize films. These temperature dependent changes in microstructure, optical transparence and electronic performance under identical low concentration condition are first linked here which are critical to understanding and optimizing SnO_2 films for next generation gas sensors, UV detectors, and transparent electronics.

2. Fabrication of SnO_2 Thin Films

2.1 Preparation of SnO_2 Thin Films

Thin films of tin dioxide (SnO_2) were prepared by the chemical thermal decomposition (CTD) technique using 0.02 M aqueous solution of tin (II) chloride dihydrate ($SnCl_2 \cdot 2H_2O$) as precursor solution. Tin(II) has a molecular weight of 225.63 g/mol and purity of 99.98% obtained from Oxford Lab Chem (India). Additionally, copper(II) chloride dihydrate ($CuCl_2 \cdot 2H_2O$), with a molecular weight of 170.48 g/mol and purity of 99%, was purchased from Alpha Chemika and reserved for future doping experiments. Double distillated water was used to dissolve the precursor salt, and the solution was then magnetically stirred for 30 minutes to completely homogenize the material.

Prior to deposition, the glass substrates were thoroughly cleaned by sequential ultrasonication in acetone, ethanol, and deionized water, each for 10 min, and finally dried in ambient air. The cleaned substrates were then heated and maintained at controlled surface temperatures of 325 °C, 350 °C, and 375 °C during the deposition process.

The precursor solution was sprayed onto the heated substrates using a fine atomizing nozzle positioned at a fixed distance of 25 cm from the substrate. The spray flow rate was maintained at 1.5 mL/min, ensuring uniform delivery of the precursor solution. In-situ decomposition of the precursor was enabled by the excess thermal energy from the substrate surface to directly form SnO_2 thin films without an additional annealing process.

The samples were naturally allowed to cool to room temperature following deposition. The resulting films had good surface uniformity, strong adhesion to the substrate, and high optical transparency. Depending on the substrate temperature, the film thicknesses were estimated to be in the range of 200 to 300 nm.

2.2 Structural and Morphological Characterization

X-ray diffraction (XRD) analysis was carried out using a Philips XRD diffractometer (Model 1730 PW, Holland) for obtaining structural properties of SnO_2 thin films by using a diffractometer fitted with Cu-Kα radiation (λ = 1.5406 Å) under an accelerated voltage of 40 kV and current of 30 mA. The 2θ range of 20° and 80° was recorded for the diffraction patterns.

Using the Debye–Scherrer equation the average crystallite size (D) was calculated [19]:

$$D = \frac{K\lambda}{\beta \cos\theta} \qquad (1)$$

Where:

- D is the crystallite size (nm),
- K is the shape factor (typically 0.9),
- λ is the X-ray wavelength (1.5406 Å),
- β is the full width at half maximum (FWHM) in radians,
- θ is the Bragg angle.

The dislocation density (δ) was estimated using [20]:

$$\delta = \frac{1}{D^2} \qquad (2)$$

The number of crystallite layers (N_L) in the film was evaluated using [21]:

$$N_L = \frac{t}{D} \qquad (3)$$

Where t is the film thickness.

The total number of crystallites across the film's thickness (N_o) was determined using [20]:

$$N_o = \frac{t}{D^3} \qquad (4)$$

The microstrain (ε) in the films was calculated from the following formulation [22]:

$$\varepsilon = \frac{\beta \cos\theta}{4} \qquad (5)$$

Scanning Electron Microscopy (SEM) was used to study the surface morphology and observe the way grains were shaped, how their sizes were distributed, and what the surface looked like.

Surface morphology was examined using a TESCAN MIRA 3 scanning electron microscope (Czech Republic). In addition, the surface roughness (R_a) and three-dimensional topographic maps of the films were obtained using a JPK NanoWizard II AFM system from Bruker (Germany), operated in tapping mode.

2.3 Optical Measurements

The UV–Vis spectrophotometer, using a PerkinElmer UV–Vis Double Beam Spectrophotometer, was used to observe the optical properties of the thin films in the wavelength range of 300–900 nm. Absorbance (A) and transmittance (T%) were measured, and from them we calculated the absorption coefficient (α) and the optical band gap energy (E_g) by using Tauc's relation. Furthermore, the refractive index (n) and the extinction coefficient (k) were found by using equations taken from Fresnel's laws and dispersion theory.

The absorption coefficient (α) was calculated using [23]:

$$\alpha = \frac{2.303\,A}{t} \qquad (6)$$

Where:

- A is the absorbance,
- t is the film thickness (in cm),
- α is the absorption coefficient (cm^{-1}).

The optical band gap (E_g) was determined from Tauc's relation [24]:

$$(\alpha h\nu)^m = B_o\left(h\nu - E_g\right) \qquad (7)$$

Where:

- $h\nu$ is the photon energy (eV),
- B_o is a constant,
- m denotes the type of optical transition (m = ½ for direct allowed transitions, m = 2 for indirect allowed transitions).

The extinction coefficient (k) was calculated using [25]:

$$k = \frac{\lambda \alpha}{4\pi} \qquad (8)$$

The refractive index (n) was calculated using reflectance data (R) and the extinction coefficient (k) [26]:

$$n = \left\{ \left[\left(\frac{1+R}{1-R} \right)^2 - k^2 \right]^{1/2} + \left(\frac{1+R}{1-R} \right) \right\} \qquad (9)$$

2.4 Electrical Characterization

Using the van der Pauw configuration, the electrical properties of SnO_2 thin films were measured at room temperature by means of Hall effect measurements using a Keithley 2182A Nano-voltmeter. The Hall measurement system was used to apply a constant 0.55 T magnetic field.

The Hall coefficient (R_H) was calculated using [27]:

$$R_H = \frac{V_H}{I_x} \cdot \frac{t}{B_z} \qquad (10)$$

Where:

- V_H is the Hall voltage (V),
- I_x is the applied current in the x-direction (A),
- t is the film thickness (cm),
- B_z is the magnetic field strength (T).

Carrier mobility (μ) was calculated using the relation [27]:

$$\mu = \sigma R_H \qquad (11)$$

Where:

- σ is the electrical conductivity (S/cm),
- μ is the carrier mobility ($cm^2/V \cdot s$).

Carrier concentration (n), resistivity (ρ), and other related parameters were determined accordingly to assess the influence of deposition temperature on the films' electronic performance.

3. Results and discussion

3.1 X-ray Diffraction Analysis

The structural characteristics of SnO_2 thin films prepared at three different substrate temperatures—325 °C, 350 °C, and 375 °C—using the chemical thermal decomposition (CTD) method at a precursor concentration of 0.02 M were investigated via X-ray diffraction (XRD). The XRD patterns are displayed in Figure 1.

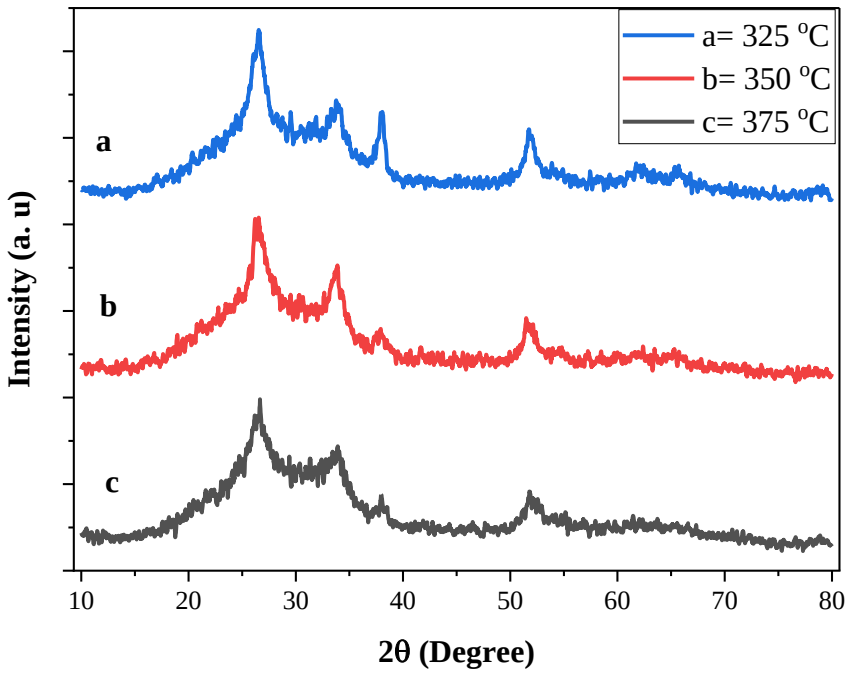

Figure 1: X-ray diffraction (XRD) patterns of SnO_2 thin films synthesized at 325 °C (blue), 350 °C (red), and 375 °C (black). All samples exhibit the rutile tetragonal phase of SnO_2. Peak intensity and sharpness decrease with increasing deposition temperature, indicating reduced crystallinity and increased structural disorder

All detected peaks correspond to the rutile SnO_2 phase, with no significant 2θ shift across the temperature range, suggesting phase stability. However, the diffraction peak intensity decreases and broadens at higher temperatures, particularly at 375 °C, indicating reduced crystallite size and increasing microstructural defects. This trend is attributed to thermal effects such as grain coalescence and lattice distortion at elevated temperatures. Conversely, at 325 °C, sharper peaks imply better crystallinity and more ordered grain growth. These structural trends are in agreement with previous reports [28].

The crystallite size (D) was calculated using the Debye–Scherrer equation based on the FWHM values of major diffraction peaks. The results are summarized in Table 1.

Table 1.

Table 1: Effect of deposition temperature on crystallite size and diffraction parameters of SnO_2 thin films.

Temperature (°C)	hkl Plane	2θ (°)	FWHM (rad)	D (nm)
325	(110)	26.37	6.135	1.45
	(101)	33.49	4.417	2.16
	(200)	37.96	1.035	9.74
	(211)	51.91	1.890	6.81
				5.04 (avg)
350	(110)	26.55	10.773	0.82
	(101)	33.77	2.145	0.82
	(200)	37.83	1.370	4.46
	(220)	51.89	3.049	6.48
				4.05 (avg)
375	(110)	26.58	7.237	1.23
	(101)	33.54	4.093	2.33
	(200)	40.99	347.75	0.03

Temperature (°C)	hkl Plane	2θ (°)	FWHM (rad)	D (nm)
	(211)	52.12	1.836	7.05
				2.62 (avg)

The data reveal a clear reduction in average crystallite size with increasing temperature. Films deposited at 325 °C exhibited the largest average size (5.04 nm), while those at 375 °C showed the smallest (2.62 nm). Although some growth improvement is evident at 350 °C (e.g., regular crystal planes), high thermal input at 375 °C causes significant peak broadening, indicating partial structural collapse or formation of defects [29].

Further microstructural analysis, including microstrain (ε), dislocation density (δ), number of crystallites per unit volume (N_o), and number of crystallite layers (NL), is presented in Table 2.

Table 2: Structural parameters of SnO_2 thin films at different deposition temperatures

Temperature (°C)	2θ (°)	Microstrain (ε)	Dislocation Density (δ, nm^{-2})	No (nm^{-2})	NL (layers)
325	26.55	0.04575	1.4715	714.00	485.22
	33.77	0.00895	0.05035	4.52	89.76
	37.83	0.00582	0.02380	1.47	61.71
	51.91	0.00974	0.03719	2.87	77.14
350	26.37	0.02607	0.47882	132.53	276.79
	33.49	0.01846	0.21502	39.88	185.48
	37.96	0.00427	0.01055	0.43	41.08

Temperature (°C)	2θ (°)	Microstrain (ε)	Dislocation Density (δ, nm^{-2})	No (nm^{-2})	NL (layers)
	51.91	0.00741	0.02153	1.26	58.70
	26.58	0.03073	0.66364	216.25	325.86
375	33.54	0.01710	0.18442	31.68	171.78
	40.99	1.42128	1091.53	1.44×10^7	13215.34
	52.12	0.00720	0.02014	1.14	56.76

At 325 °C, the films exhibit significant internal strain and high dislocation density, implying the presence of lattice imperfections due to constrained crystal growth. Raising the temperature to 350 °C results in a marked reduction in microstrain and defect density, supporting the hypothesis that this is an optimal temperature for promoting crystallinity and reducing structural stress.

However, further temperature increase to 375 °C induces structural degradation, as evidenced by a sharp increase in strain (ε = 1.42128) and dislocation density (δ = 1091.53 nm^{-2}) in some orientations. The observed spike in crystallite count and layering (NL = 13215) implies disordered nano-domain formation, potentially due to excessive evaporation and uncontrolled grain boundary rearrangement [30].

In summary, XRD analysis demonstrates that 350 °C provides the best compromise between enhanced grain growth and minimal structural defect generation, making it a favorable condition for the fabrication of high-quality SnO_2 thin films for optoelectronic applications.

3.2 FE-SEM Analysis Results

Figure 2 (a-c) displays the field emission scanning electron microscopy (FE-SEM) images of SnO_2 thin films synthesized at a molar concentration of 0.02 M and deposited at varying substrate temperatures: 325 °C, 350 °C, and 375 °C, respectively. These morphological

observations provide strong corroborative evidence for the structural evolution trends previously observed in the X-ray diffraction (XRD) analysis.

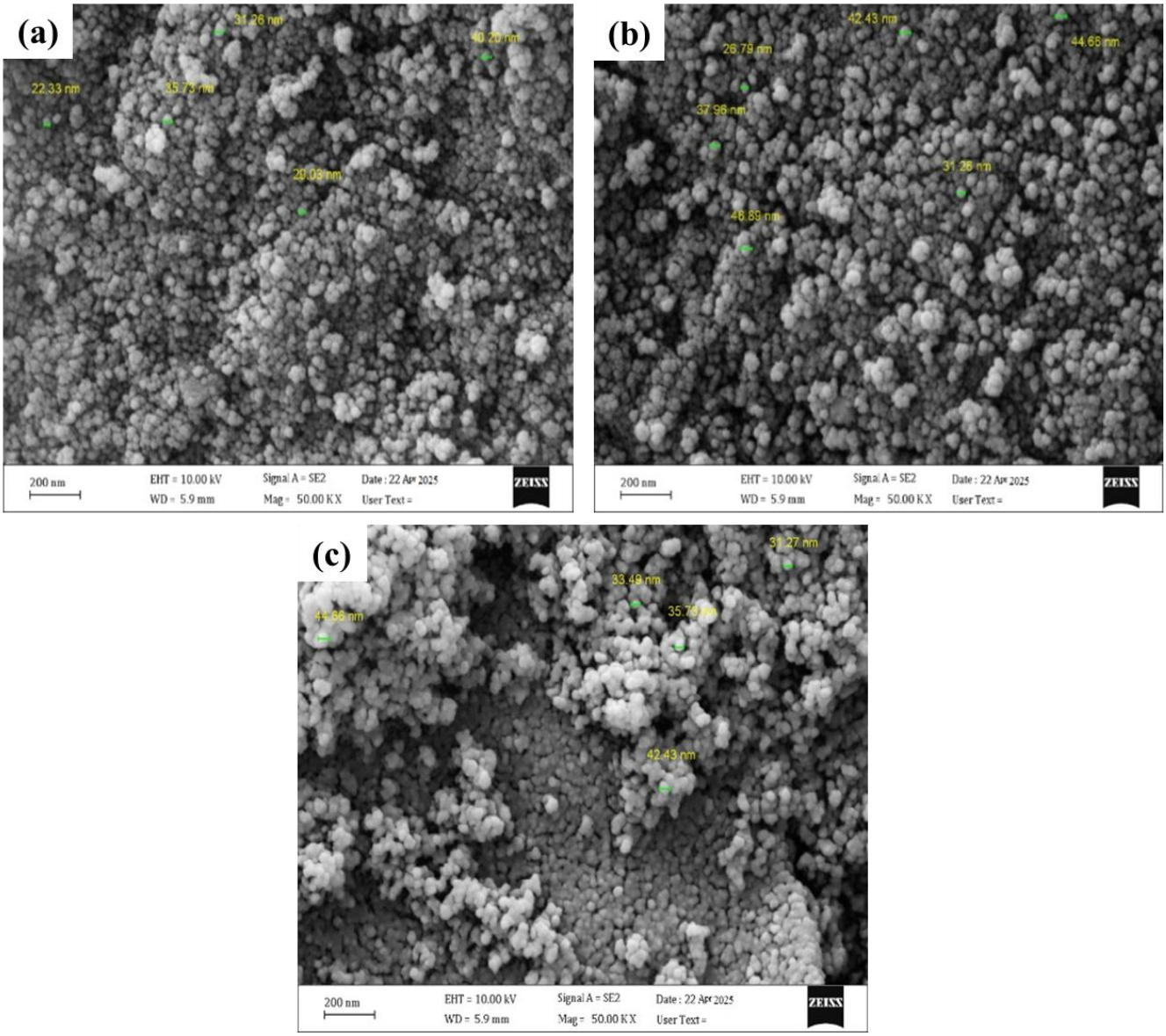

Figure 2: FE-SEM images of SnO_2 thin films deposited at (a) 325 °C, (b)350 °C, and (c) 375 °C using the chemical thermal decomposition method at a concentration of 0.02 M.

At 325 °C, the FE-SEM image reveals a structurally disordered surface composed of non-uniform and loosely packed nanoparticles. Heterogeneous clusters and intergranular voids dominate the film morphology, indicating limited crystallite connectivity and incomplete grain growth. This aligns well with the XRD results, which showed relatively higher microstrain and dislocation density, as well as smaller and defect-rich crystallites at this temperature. The

insufficient thermal energy likely hindered atomic mobility, resulting in poor grain coalescence and increased structural porosity.

When the deposition temperature was increased to 350 °C, a notable morphological improvement occurred. The grains became more uniform in size and distribution, with a denser, smoother surface and significantly reduced porosity. This microstructural refinement is consistent with the XRD findings, where reduced FWHM values and improved crystallite size uniformity indicated enhanced crystallinity. Moreover, the substantial decrease in both microstrain and dislocation density at this temperature confirms a reduction in internal stresses and defects, supporting the development of a more ordered nanocrystalline framework.

Further increasing the temperature to 375 °C resulted in continued grain growth and surface densification, as evident in the more compact microstructure and slightly larger grains seen in the SEM image. However, localized coalescence and excessive atomic diffusion may have introduced new structural instabilities. This is reflected in the XRD analysis by the irregular behavior of microstrain and dislocation density, particularly the spike in crystallographic defects and abnormally high crystallite count at specific orientations. These phenomena suggest that while 375 °C promotes grain enlargement, it may also induce undesirable thermally activated lattice deformations, compromising the uniformity of the crystalline matrix.

In conclusion, the FE-SEM observations reinforce the XRD analysis by visually confirming the thermal dependence of grain formation, crystallite arrangement, and surface compactness. The optimal temperature of 350 °C offers a well-balanced condition where structural ordering and surface densification are simultaneously achieved, making it a favorable setting for high-performance SnO_2 thin film fabrication.

3.3 AFM Analysis Results

Figure 3 (a-c) illustrates the atomic force microscopy (AFM) images of SnO_2 thin films prepared via the chemical thermal decomposition method at a precursor concentration of 0.02 M and deposited at three different substrate temperatures: 325 °C, 350 °C, and 375 °C, receptively. The AFM results provide further insight into the surface morphology and nanostructure uniformity observed earlier in the FE-SEM analysis.

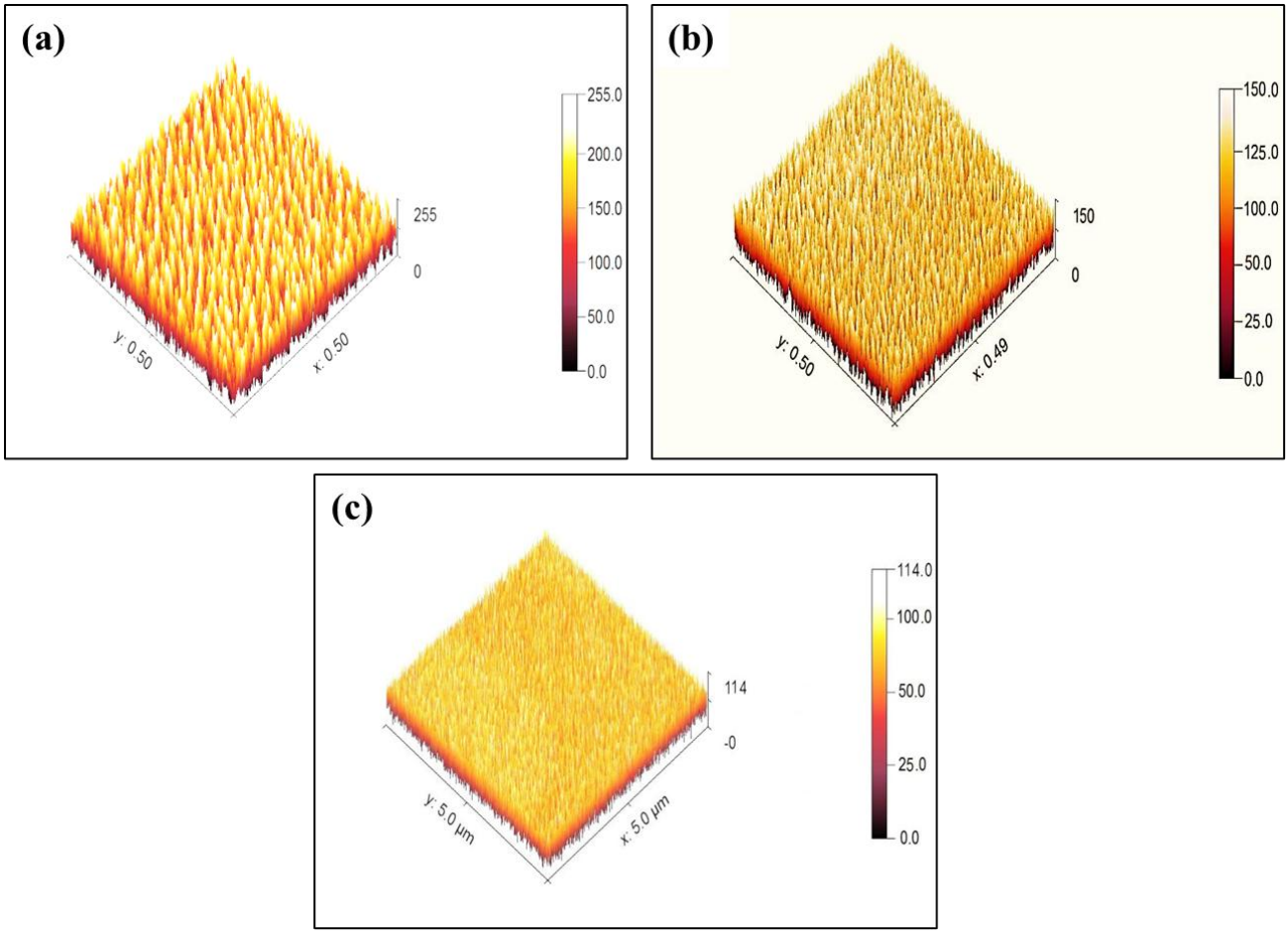

Figure 3: Atomic force microscopy (AFM) images of SnO_2 thin films synthesized at (a) 325 °C, (b) 350 °C, and (c) 375 °C, showing temperature-dependent changes in surface topography.

As summarized in Table 3, a clear thermal influence on the surface topography is evident. At 325 °C, the film exhibited a relatively rough surface with an average grain size of 51.26 nm and a mean surface roughness (Ra) of 42.15 nm. The maximum height variation reached 255 nm, indicating significant height disparities likely caused by disordered grain formation and surface porosity. These results are in line with both SEM and XRD findings, which showed incomplete crystallite formation and high dislocation density at this temperature.

At 350 °C, improved thermal conditions contributed to a more regular grain growth mechanism. The grain size decreased to 43.51 nm, while the roughness and height variation reduced to 36.71 nm and 150 nm, respectively. This reduction in surface roughness suggests enhanced atomic diffusion and grain boundary refinement, promoting a more compact and uniform film surface. These observations are consistent with the XRD data, which demonstrated reduced

microstrain and improved crystallinity at 350 °C, marking this as the optimal growth temperature.

Table 3: AFM-derived surface topography parameters of SnO_2 thin films prepared at different substrate temperatures.

Temperature (°C)	Average Grain Size (nm)	Maximum Height (nm)	Mean Roughness (Ra, nm)
325	51.26	255	42.15
350	43.51	150	36.71
375	16.61	114	13.51

Further increasing the temperature to 375 °C resulted in a dramatic improvement in surface smoothness. The average grain size significantly decreased to 16.61 nm, the surface roughness dropped to 13.51 nm, and the maximum height was only 114 nm. This level of smoothness and homogeneity is indicative of enhanced recrystallization and atomic rearrangement processes, which favor the formation of a well-aligned nanolayer with minimal topographic defects [31]. These results reinforce the earlier inference that higher thermal input facilitates improved nanostructural order; however, the XRD analysis also cautioned that beyond optimal temperature, localized lattice distortions may begin to emerge.

In conclusion, AFM analysis confirms the direct correlation between deposition temperature and surface quality of SnO_2 thin films. The optimal balance between grain size uniformity and surface smoothness was achieved at 375 °C, although structural perfection peaked at 350 °C. These findings support the complementary conclusions derived from XRD and FE-SEM analyses.

3.4 Optical analysis results

Figure 4 presents the optical transmittance spectra of SnO_2 thin films prepared at a precursor concentration of 0.02 M and deposited at various substrate temperatures (325 °C, 350 °C, and 375 °C) using the chemical pyrolysis method. The spectra were recorded in the UV–Visible region and exhibit a clear temperature-dependent variation in transmittance.

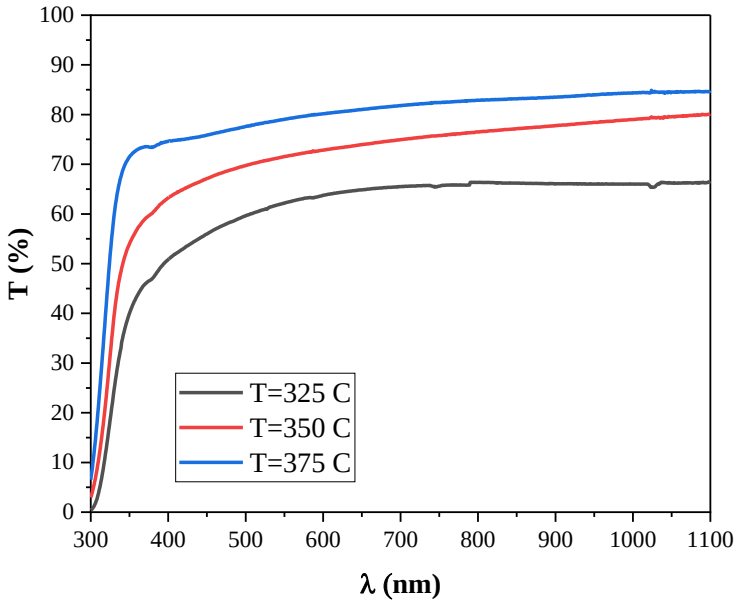

Figure 4: UV–Vis transmittance spectra of SnO_2 thin films synthesized at 325 °C, 350 °C, and 375 °C using the chemical pyrolysis method with a precursor concentration of 0.02 M

As the deposition temperature increased, a notable enhancement in optical transmittance was observed across the entire spectral range. The sample prepared at 325 °C exhibited an average transmittance of approximately 45.5%, whereas films deposited at 350 °C and 375 °C showed transmittance values of about 61.3% and 75.8%, respectively. This progressive increase in transmittance with temperature is attributed primarily to a reduction in film thickness and surface scattering losses, which often result from improved surface morphology and densification at higher temperatures.

These results correlate well with the FE-SEM and AFM findings, which indicated enhanced grain alignment and reduced surface roughness as temperature increased. The formation of a smoother and more compact microstructure at elevated temperatures reduces light absorption and scattering, thereby promoting higher optical transmission. Moreover, reduced defect states and improved crystallinity, as confirmed by XRD, further support the enhanced optical transparency.

The observed trends are consistent with findings reported in previous studies [32, 33], affirming that optimized deposition temperature enhances the optical clarity of SnO_2 thin films, making them suitable for applications in transparent optoelectronic devices.

Figure 5 shows the absorption coefficient (α) spectra of SnO_2 thin films deposited at different substrate temperatures (325 °C, 350 °C, and 375 °C) using the thermochemical decomposition method (Equation 6) with a precursor concentration of 0.02 M.

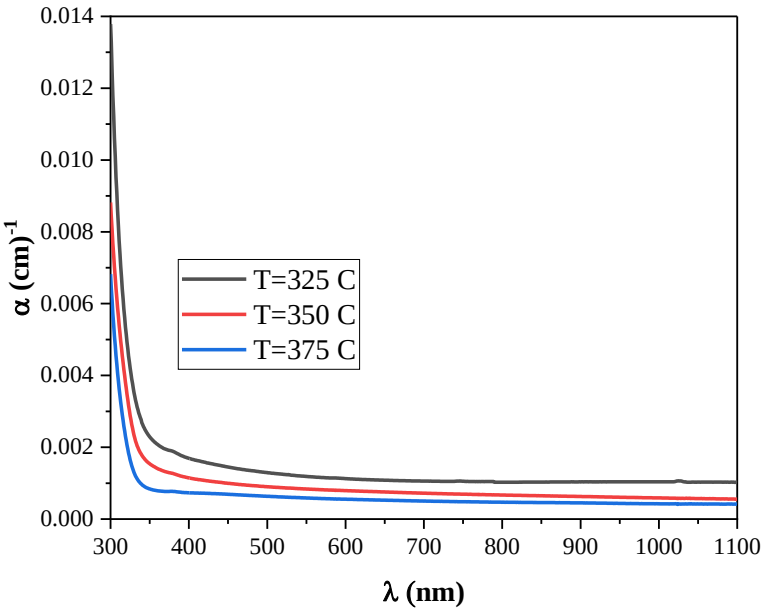

Figure 5: Absorption coefficient spectra of SnO_2 thin films synthesized at 325 °C, 350 °C, and 375 °C via the thermochemical decomposition method at a precursor concentration of 0.02 M

The results reveal a clear inverse relationship between substrate temperature and absorption coefficient. As the deposition temperature increased, the overall absorption of the films decreased noticeably. The film prepared at 325 °C exhibited the highest absorption across the visible spectrum, whereas the sample synthesized at 375 °C displayed the lowest absorption, particularly in the 400–800 nm range. This trend is consistent with the transmittance behavior shown in Figure 4, further confirming that films grown at higher temperatures become more optically transparent.

The decrease in absorption with increasing temperature can be attributed to enhanced film quality and reduced optical scattering, which result from improved crystallinity and a smoother, more uniform surface morphology. As observed in the AFM and SEM results, elevated temperatures facilitate better atomic arrangement and grain boundary minimization, leading to reduced defect density and lower light absorption. Additionally, the higher oxidation efficiency

at 375 °C promotes stoichiometric film formation, which further contributes to reduced sub-bandgap absorption.

These results collectively affirm that high-temperature deposition conditions are favorable for producing SnO_2 films with lower optical losses and higher transparency, suitable for optoelectronic and window-layer applications.

Figure 6 illustrates the Tauc plots $(\alpha h\nu)^2$ versus $h\nu$ for SnO_2 thin films synthesized at different deposition temperatures (325 °C, 350 °C, and 375 °C) using the thermochemical decomposition method with a precursor concentration of 0.02 M. The plots exhibit a linear dependence in the high-energy region, confirming that the films possess a direct allowed band gap.

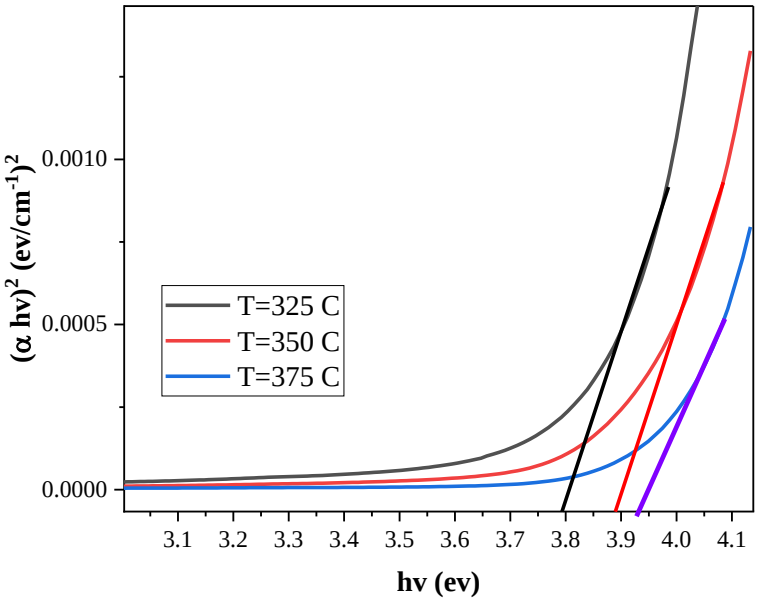

Figure 6: Tauc plots (αhν)2 vs. hν for SnO_2 thin films prepared at 325 °C, 350 °C, and 375 °C. The plots reveal a direct band gap nature, with the energy gap increasing from 3.80 eV to 3.94 eV as deposition temperature rises.

The optical band gap energies (E_g) were determined by extrapolating the linear region of each curve to the photon energy axis where $(\alpha h\nu)^2 = 0$. The estimated energy gap values were:

- 3.80 eV for the film deposited at 325 °C,
- 3.88 eV at 350 °C,

- 3.94 eV at 375 °C.

An increasing trend in E_g with rising deposition temperature is observed. This shift can be attributed to multiple temperature-induced effects. Firstly, the improvement in crystallinity and reduction in structural defects at higher temperatures—confirmed by XRD and AFM results—leads to sharper band edges and reduced localized states. Secondly, the observed widening of the band gap is consistent with the Burstein–Moss effect, where increased carrier concentration and filling of lower energy conduction states result in an apparent blue shift of the optical absorption edge.

Additionally, subtle lattice distortion and internal strain, particularly at 375 °C, may also contribute to the observed band gap expansion by altering the electronic structure of the SnO_2 lattice [34].

These findings support the conclusion that higher thermal treatment enhances both the structural integrity and optical quality of SnO_2 thin films, making them promising candidates for transparent optoelectronic and UV filtering applications.

Figure 7 presents the refractive index (nnn) values of SnO_2 thin films synthesized via the chemical pyrolysis method at a molar concentration of 0.02 M and at different substrate temperatures: 325 °C, 350 °C, and 375 °C. The refractive index was calculated using reflectance data and the extinction coefficient based on Fresnel's relations.

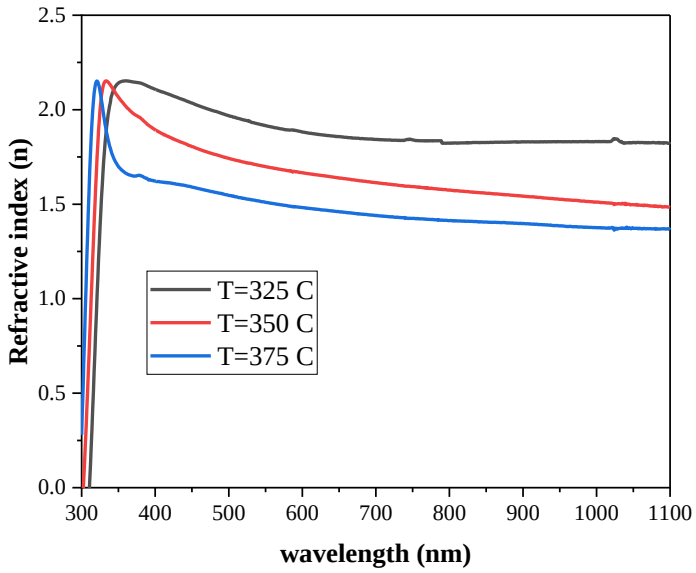

Figure 7: Refractive index (nnn) values of SnO_2 thin films prepared at 325 °C, 350 °C, and 375 °C by the chemical pyrolysis method at a precursor concentration of 0.02 M.

As shown, the refractive index of the film decreases with increasing deposition temperature. Specifically:

- The film deposited at 325 °C exhibited a refractive index of approximately 2.2.
- At 350 °C, the index decreased to 1.9.
- At 375 °C, it further declined to 1.7.

This reduction in refractive index is commonly attributed to an increase in porosity and reduced packing density of the film as the growth temperature increases. Although higher temperatures generally improve crystallinity (as seen in the XRD results), they may also promote the formation of voids or columnar structures, which reduce the film's effective optical density.

The trend is also consistent with the AFM and SEM results, which revealed smoother surfaces and increased uniformity at higher temperatures—conditions often associated with reduced refractive index due to decreased light scattering and lower dielectric contrast. Additionally, as the band gap widened with temperature, the material's electronic polarizability may also decrease, further contributing to the observed reduction in nnn.

These findings align with prior literature [35], where refractive index reduction was linked to both enhanced porosity and thermally induced changes in microstructure.

Figure 8 presents the extinction coefficient (kkk) as a function of wavelength for SnO_2 thin films prepared via the thermochemical decomposition method at a concentration of 0.02 M and substrate temperatures of 325 °C, 350 °C, and 375 °C.

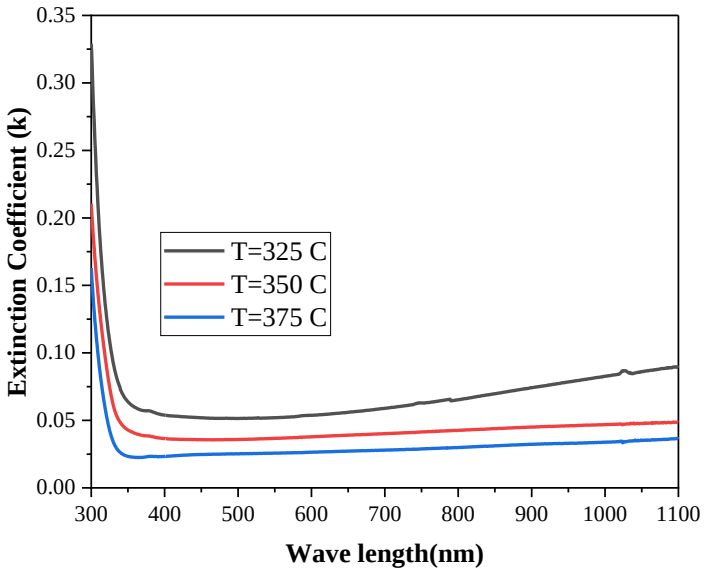

Figure 8: Extinction coefficient (kkk) versus wavelength for SnO_2 thin films synthesized at 325 °C, 350 °C, and 375 °C using the thermochemical decomposition method

Across all temperatures, the SnO_2 films exhibit low extinction coefficient values, confirming their high transparency throughout the visible and near-infrared regions. This transparency is consistent with earlier findings in the transmittance and absorption coefficient analyses, where reduced absorbance and enhanced transmittance were observed with increasing temperature.

A distinct blue shift in the absorption edge is also evident in the extinction coefficient spectra as the preparation temperature increases. This shift corresponds to the earlier observed band gap widening and is attributed to the Burstein–Moss effect and thermally induced improvements in crystallinity. The sharper absorption edge at 375 °C further supports the presence of fewer defect states and improved optical quality.

Moreover, the extinction coefficient values tend to stabilize beyond 600 nm, particularly for the higher temperature samples, indicating reduced sub-bandgap absorption and minimal scattering losses. These findings align with those reported in [36], where extinction coefficient stability was associated with enhanced microstructural ordering and reduced impurity levels.

In summary, the extinction coefficient data reinforce the conclusion that increasing deposition temperature enhances the optical transparency and sharpness of the absorption edge in SnO_2 thin films, making them highly suitable for transparent electronics and optoelectronic windows.

3.5 Electrical analysis results

Electrical properties of the SnO_2 thin films were investigated through Hall effect measurements conducted at room temperature using the van der Pauw configuration. The results, including Hall coefficient, carrier concentration, mobility, resistivity, and conductivity, are summarized in Table 4. The measurements reveal a strong dependence of electrical behavior on the substrate temperature during film deposition.

Table 4. Hall effect measurements and electrical properties of SnO_2 thin films synthesized at different temperatures.

T (°C)	Type	Hall Coefficient R_H (m^2/C)	Carrier Concentration n (cm^{-3})	Mobility μ ($cm^2/V{\cdot}s$)	Resistivity ρ ($\Omega{\cdot}cm$)	Conductivity σ ($\Omega^{-1}{\cdot}cm^{-1}$)
325	n-type	-1.150×10^4	5.45×10^{14}	2.772×10^3	5.37×10^2	1.86×10^{-3}
350	n-type	-1.178×10^5	6.212×10^{13}	4.257×10^3	2.273×10^1	3.651×10^{-2}
375	n-type	-1.828×10^4	3.614×10^{14}	5.968×10^1	3.423×10^2	2.52×10^{-3}

The negative values of the Hall coefficient (RH = − 1.150 × 10^4, − 1.178 × 10^5, and − 1.828 × 10^4 m^2/C) confirm that the dominant charge carriers in all samples are electrons, indicating n-type conductivity. Variations in the magnitude of R_H with increasing temperature reflect changes in carrier concentration and scattering mechanisms. Specifically, the reduced absolute value of R_H at 375 °C compared to 350 °C implies a higher free electron concentration, which is characteristic of increased thermal activation and oxygen vacancy generation, consistent with prior findings [37].

Carrier concentration values were found to vary significantly with processing temperature:

- 5.45 × 10^{14} cm^{-3} at 325 °C
- 6.212 × 10^{13} cm^{-3} at 350 °C
- 3.614 × 10^{14} cm^{-3} at 375 °C

The highest carrier concentration occurred at 375 °C, suggesting enhanced thermal excitation and possible increase in oxygen vacancies or interstitial Sn atoms. Conversely, the drop at 350 °C may be attributed to enhanced crystallinity and reduced defect-related donor states, as observed in the XRD and AFM results. These observations are consistent with prior literature on temperature-dependent defect chemistry in tin oxide [38].

The carrier mobility values exhibited a distinct temperature-dependent trend:

- 2.772 × 10^3 cm^2/V·s at 325 °C
- 4.257 × 10^3 cm^2/V·s at 350 °C
- 5.968 × 10^1 cm^2/V·s at 375 °C

Maximum mobility was observed at 350 °C, indicating that this temperature promotes optimal crystallinity with minimal grain boundary and defect scattering. The sharp decline in mobility at 375 °C, despite higher carrier concentration, suggests that carrier scattering due to grain boundary imperfections or structural dislocations limits transport efficiency. These results are in agreement with the microstructural analysis and findings in [39].

The resistivity values showed that the film deposited at 350 °C had the lowest resistivity:

- 5.37 × 10^2 Ω·cm at 325 °C

- 2.273×10^{1} Ω·cm at 350 °C
- 3.423×10^{2} Ω·cm at 375 °C

This result indicates enhanced electron transport at 350 °C, supported by the observed high mobility and moderate carrier concentration. The increased resistivity at 375 °C is attributed to increased carrier scattering, despite higher carrier density, which reduces net conductivity. These findings confirm the complex interplay between crystallinity, carrier dynamics, and temperature treatment, as supported by previous studies [40].

Electrical conductivity, the reciprocal of resistivity, followed the expected trend:

- $1.86 \times 10^{-3}\ \Omega^{-1}\cdot cm^{-1}$ at 325 °C
- $3.651 \times 10^{-2}\ \Omega^{-1}\cdot cm^{-1}$ at 350 °C
- $2.52 \times 10^{-3}\ \Omega^{-1}\cdot cm^{-1}$ at 375 °C

The film deposited at 350 °C exhibited the highest electrical conductivity due to the combined effect of optimal mobility and adequate carrier concentration. At 375 °C, although electron density increased, the reduced mobility severely limited conductivity. This emphasizes that mobility, strongly influenced by crystal quality, is equally as critical as carrier concentration in determining electrical performance. These observations are consistent with the conclusions of [41].

4. Conclusions

This study demonstrated that preparation temperature plays a pivotal role in determining the structural, optical, and electrical properties of SnO_2 thin films synthesized via the chemical pyrolysis method at a precursor concentration of 0.02 M.

Among the investigated temperatures, 350 °C yielded the most favorable microstructural characteristics, including enhanced crystallinity, reduced microstrain, lower dislocation density, and well-defined grain morphology. These features contributed to improved surface homogeneity, as confirmed by SEM and AFM analyses.

From an electrical perspective, the film deposited at 350 °C exhibited the highest electrical conductivity and lowest resistivity, supported by optimal carrier mobility and balanced electron

concentration. This reflects a highly ordered lattice with minimal carrier-scattering sites, enabling efficient charge transport.

Although increasing the temperature to 375 °C further enhanced transmittance and widened the optical band gap—due to reduced film thickness and increased porosity—it also introduced excessive crystalline defects, leading to a significant drop in carrier mobility despite higher electron concentration. This degradation in electrical performance highlights the importance of controlling thermal processing to preserve structural coherence.

In conclusion, 350 °C represents the optimal deposition temperature for producing high-quality SnO_2 thin films with a well-balanced combination of structural integrity, optical transparency, and electrical conductivity. These properties make such films particularly suitable for applications in gas sensing, transparent electronics, and micro-optical devices.

Statements and Declarations

Funding

The authors declare that no funds, grants, or other support were received during the preparation of this manuscript.

Competing Interests

The authors have no relevant financial or non-financial interests to disclose.

Author Contributions

All authors contributed to the study conception and design. Material preparation, data collection, and analysis were performed by Ibtihaj Abdulsamad Sabri and Jamal Fadhil Mohammad. The first draft of the manuscript was written by Ibtihaj Abdulsamad Sabri, and both authors commented on previous versions of the manuscript. All authors read and approved the final manuscript.

Data Availability Statement

The datasets generated and/or analyzed during the current study are available from the corresponding author upon reasonable request.

References

[1] E. Klaus, M. Rainald, and S. Stefan, "Metallic Oxides (ITO, ZnO, SnO2 , TiO2)," in *Transparent Conductive Materials: Materials, Synthesis, Characterization, Applications*: Wiley, 2018, pp. 31-80.

[2] N. Salah, W. M. Al-Shawafi, S. S. Habib, A. Azam, and A. Alshahrie, "Growth-controlled from SnO2 nanoparticles to SnO nanosheets with tunable properties," *Materials & Design*, vol. 103, pp. 339-347, 2016/08/05/ 2016, doi: https://doi.org/10.1016/j.matdes.2016.04.092.

[3] R. Achour, S. Benramache, and B. Boubaker, "Preparation of n-type semiconductor SnO2 thin films," *Journal of Semiconductors*, vol. 34, p. 083002, 08/01 2013, doi: 10.1088/1674-4926/34/8/083002.

[4] P. Lisnic, L. Hrostea, L. Leontie, and M. Girtan, "Fluorine-Doped SnO 2 Thin Films in Solar Cell Applications. Morphological, Optical and Electrical Properties," *Archives of Metallurgy and Materials*, 2023-06-06 2023, doi: 10.24425/amm.2023.142426.

[5] S. Akinsola, K. Adedayo, A. Alabi, D. Olanrewaju, A. Ajayi, and O. Babalola, "Spray Pyrolysed Nanostructured Gold-Doped Tin Oxide (Auto) Thin Films," *Journal of Applied Sciences and Environmental Management*, 2021-10-08 2021, doi: 10.4314/jasem.v25i4.12.

[6] N. Sharma, B. Sharma, S. Das, P. Chettri, P. Karki, R. Pradhan, B. Chettri, and A. Rao, "A First-Principle Study to Investigate Electrical and Optical Properties of Tin Oxide," *2024 IEEE International Conference of Electron Devices Society Kolkata Chapter (EDKCON)*, pp. 573-577, 2024-11-30 2024, doi: 10.1109/EDKCON62339.2024.10870789.

[7] C. Falcony, M. A. Aguilar-Frutis, and M. García-Hipólito, "Spray Pyrolysis Technique; High-K Dielectric Films and Luminescent Materials: A Review," *Micromachines*, vol. 9, no. 8, p. 414, 2018. [Online]. Available: https://www.mdpi.com/2072-666X/9/8/414.

[8] A. B. Workie, H. S. Ningsih, and S.-J. Shih, "An comprehensive review on the spray pyrolysis technique: Historical context, operational factors, classifications, and product applications," *Journal of Analytical and Applied Pyrolysis*, vol. 170, p. 105915, 2023/03/01/ 2023, doi: https://doi.org/10.1016/j.jaap.2023.105915.

[9] R. Udayakumar, "Synthesis and Structural Characterization of Thin Films of SnO2 Prepared by Spray Pyrolysis Technique," *Indian journal of science and technology*, vol. 6, pp. 1-4, 2013-12-20 2013, doi: 10.17485/ijst/2013/v6isp6.19.

[10] T. Zinchenko, E. Pecherskaya, and D. Artamonov, "The properties study of transparent conductive oxides (TCO) of tin dioxide (ATO) doped by antimony obtained by spray pyrolysis," *AIMS Materials Science*, 2019-03-24 2019, doi: 10.3934/MATERSCI.2019.2.276.

[11] Solís, Peinado, R. Barrado, Martín, and Parra, "Tin dioxide transparent films sprayed from different precursors for supercapacitor current collectors," *Applied Physics A*, vol. 128, 2022-02-11 2022, doi: 10.1007/s00339-022-05337-y.

[12] E. Turan, M. Kul, and S. Akın, "Structural and optical investigation of spray-deposited SnO2 thin films," *Journal of Materials Science: Materials in Electronics*, vol. 33, pp. 15689-15703, 2022-06-08 2022, doi: 10.1007/s10854-022-08472-7.

[13] A. Lateef, S. Mohameed, and F. Mostafah, "Study on effect of thickness and temperature of SnO2 thin film prepared by spray pyrolysis technique," *Tikrit Journal of Pure Science*, 2023-02-07 2023, doi: 10.25130/tjps.v21i4.1063.

[14] P. Hind, P. Kumar, U. Goutam, and B. Rajendra, "Impact of deposition temperature on persistent photoconductivity of SnO2 thin films deposited using spray pyrolysis technique suitable in optoelectronic synaptic devices," *Optical Materials*, 2024-07-01 2024, doi: 10.1016/j.optmat.2024.115579.

[15] S. Roguai and A. Djelloul, "Structural, morphological, optical and electrical properties of Ni-doped SnO2 thin films by pneumatic spray pyrolysis method," *Bulletin of Materials Science*, vol. 45, 2022-11-16 2022, doi: 10.1007/s12034-022-02804-3.

[16] N. Khademi, M. Bagheri-Mohagheghi, and A. Shirpay, "Bi-doped SnO2 transparent conducting thin films deposited by spray pyrolysis: structural, electrical, optical, and photo-thermoelectric properties," *Optical and Quantum Electronics*, vol. 54, pp. 1-17, 2022-02-01 2022, doi: 10.1007/s11082-022-03515-z.

[17] V. Janakiraman, V. Tamilnayagam, R. Sundararajan, S. Suresh, and C. Biju, "Structural, optical and morphological properties of Ta2O5/SnO2 nanocomposite thin film prepared by spray pyrolysis method," *Journal of Materials Science: Materials in Electronics*, vol. 32, pp. 9244-9252, 2021-03-05 2021, doi: 10.1007/s10854-021-05589-z.

[18] G. Charrada, M. Ajili, N. Jebbari, S. Bernardini, K. Aguir, and N. Kamoun, "Improvement of ozone sensing parameters by CuO–SnO2: F mixed oxide sprayed thin films," *Journal of Materials Science: Materials in Electronics*, 2024-06-01 2024, doi: 10.1007/s10854-024-12873-1.

[19] A. Monshi, M. Foroughi, and M. Monshi, "Modified Scherrer Equation to Estimate More Accurately Nano-Crystallite Size Using XRD," *World Journal of Nano Science and Engineering*, vol. 02, pp. 154-160, 2012-09-28 2012, doi: 10.4236/WJNSE.2012.23020.

[20] T. Serin, N. Serin, S. Karadeniz, H. Sarı, N. Tuğluoğlu, and O. Pakma, "Electrical, structural and optical properties of SnO2 thin films prepared by spray pyrolysis," *J. Non·Cryst. Solids*, vol. 352, no. 3, pp. 209-215, 2006/03/01/ 2006, doi: https://doi.org/10.1016/j.jnoncrysol.2005.11.031.

[21] Y. Larbah, M. Adnane, and T. Sahraoui, "Effect of substrate temperature on structural and optical properties of spray deposited ZnO thin films," *Materials Science-Poland*, vol. 33, no. 3, pp. 491-496, 2015, doi: 10.1515/msp-2015-0062.

[22] Y. Mahammed, H. S. Ali, and H. Mahammed, "Preparation and characterization of SnO_2 thin films prepared by chemical spray pyrolysis technique at different substrate temperatures," *Review of Computer Engineering Studies (RCMA)*, vol. 33, no. 5, pp. 385-390, 2023, doi: 10.18280/rcma.330505.

[23] N. Habubi and S. Chiad, "Physical characterization of sprayed SnO2 thin films," *Materials Science : an Indian Journal*, vol. 10, pp. 397-401, 01/01 2014.

[24] Ł. Haryński, A. Olejnik, K. Grochowska, and K. Siuzdak, "A facile method for Tauc exponent and corresponding electronic transitions determination in semiconductors directly from UV–Vis spectroscopy data," *Optical Materials*, 2022-05-01 2022, doi: 10.1016/j.optmat.2022.112205.

[25] R. Martín-Palma, J. Martínez-Duart, and A. Macleod, "Determination of the optical constants of a semiconductor thin film employing the matrix method," *IEEE Trans. Educ.*, vol. 43, pp. 63-68, 2000-02-01 2000, doi: 10.1109/13.825742.

[26] O. Urper, M. Tonka, and N. Baydogan, "Modification of optical constants at nanospherical ZnO:Al thin film," *Journal of Materials Science: Materials in Electronics*, vol. 34, pp. 1-11, 2023-01-25 2023, doi: 10.1007/s10854-022-09751-z.

[27] F. Gutierrez, L. Arés, J. Robla, J. Getino, M. Horrillo, I. Sayago, and J. Agapito, "Hall coefficient measurements for SnO2 doped sensors, as a function of temperature and atmosphere," *Sensors and Actuators B-chemical*, vol. 15, pp. 98-104, 1993-08-01 1993, doi: 10.1016/0925-4005(93)85034-8.

[28] D. Sukanya, D. Nathan, R. Mahesh, and P. Sagayaraj, "Comparative Studies on the Aqueous Synthesis and Biocompatibility of L-Cysteine and Mercaptopropionic Acid Capped CdSe/CdS/ZnS Core/Shell/Shell Quantum Dots," (in eng), *J Nanosci Nanotechnol*, vol. 19, no. 6, pp. 3334-3342, Jun 1 2019, doi: 10.1166/jnn.2019.16095.

[29] C. Jia, T. Dong, M. Li, P. Wang, and P. Yang, "Preparation of anatase/rutile TiO2/SnO2 hollow heterostructures for gas sensor," *Journal of Alloys and Compounds*, vol. 769, pp. 521-531, 2018/11/15/ 2018, doi: https://doi.org/10.1016/j.jallcom.2018.08.035.

[30] N. Bhakta and P. K. Chakrabarti, "XRD analysis, Raman, AC conductivity and dielectric properties of Co and Mn co-doped SnO2 nanoparticles," *Applied Physics A*, vol. 125, no. 1, p. 73, 2019/01/05 2019, doi: 10.1007/s00339-018-2370-2.

[31] A. Gaber, M. A. Abdel-Rahim, A. Y. Abdel-Latief, and M. N. Abdel-Salam, "Influence of Calcination Temperature on the Structure and Porosity of Nanocrystalline SnO2 Synthesized by a Conventional Precipitation method," *International Journal of Electrochemical Science*, vol. 9, no. 1, pp. 81-95, 2014/01/01/ 2014, doi: https://doi.org/10.1016/S1452-3981(23)07699-X.

[32] N. Bakr, S. Salman, and N. Mohammed, "ROLE OF SUBSTRATE TEMPERATURE ON THE STRUCTURAL AND OPTICAL PROPERTIES OF CHEMICALLY SPRAYED SnO 2 THIN FILMS," *Digest Journal of Nanomaterials and Biostructures*, vol. 14, pp. 517-525, 07/26 2019.

[33] R. Lotfi Orimi and M. Maghouli, "Optical characterization of SnO2 nanostructure thin films, annealed at different temperatures," *Optik*, vol. 127, no. 1, pp. 263-266, 2016/01/01/ 2016, doi: https://doi.org/10.1016/j.ijleo.2015.10.033.

[34] M. Diantoro, Kholid, A. A. Mustikasari, and Yudiyanto, "The Influence of SnO2 Nanoparticles on Electrical Conductivity, and Transmittance of PANI-SnO2 Films," *IOP Conference Series: Materials Science and Engineering*, vol. 367, no. 1, p. 012034, 2018/05/01 2018, doi: 10.1088/1757-899X/367/1/012034.

[35] O. Erken, O. M. Ozkendir, M. Gunes, E. Harputlu, C. Ulutas, and C. Gumus, "A study of the electronic and physical properties of SnO2 thin films as a function of substrate temperature," *Ceramics International*, vol. 45, no. 15, pp. 19086-19092, 2019/10/15/ 2019, doi: https://doi.org/10.1016/j.ceramint.2019.06.153.

[36] P. Chetri and A. Choudhury, "Investigation of optical properties of SnO2 nanoparticles," *Physica E: Low-dimensional Systems and Nanostructures*, vol. 47, pp. 257-263, 2013/01/01/ 2013, doi: https://doi.org/10.1016/j.physe.2012.11.011.

[37] J. Gong, X. Wang, X. Fan, R. Dai, W. Zhongping, Z. Zhang, and D. Zejun, "Temperature dependent optical properties of SnO2 film study by ellipsometry," *Optical Materials Express*, vol. 9, pp. 3691-3699, 08/13 2019, doi: 10.1364/OME.9.003691.

[38] A. Paliwal, A. Sharma, M. Tomar, and V. Gupta, "Surface plasmon resonance study on the optical sensing properties of tin oxide (SnO2) films to NH3 gas," *J. Appl. Phys.*, vol. 119, no. 16, 2016, doi: 10.1063/1.4948332.

[39] Y.-C. Ji, H.-X. Zhang, X.-H. Zhang, and Z.-Q. Li, "Structures, optical properties, and electrical transport processes of SnO2 films with oxygen deficiencies," *physica status solidi (b)*, vol. 250, no. 10, pp. 2145-2152, 2013, doi: https://doi.org/10.1002/pssb.201349086.

[40] H. Luo, L. Y. Liang, H. T. Cao, Z. M. Liu, and F. Zhuge, "Structural, Chemical, Optical, and Electrical Evolution of SnOx Films Deposited by Reactive rf Magnetron Sputtering," *ACS Applied Materials & Interfaces*, vol. 4, no. 10, pp. 5673-5677, 2012/10/24 2012, doi: 10.1021/am301601s.

[41] A. Wang, K. Bushick, N. Pant, W. Lee, X. Zhang, J. Leveillee, F. Giustino, S. Poncé, and E. Kioupakis, "Electron mobility of SnO2 from first principles," *Appl. Phys. Lett.*, vol. 124, no. 17, 2024, doi: 10.1063/5.0198885.